Structure of the dual-function fructose-1,6/sedoheptulose-1,7-bisphosphatase from *Thermosynechococcus elongatus* bound with sedoheptulose-7-phosphate

Charles A. R. Cotton, Burak V. Kabasakal, Nishat A. Miah and James W. Murray*

Department of Life Sciences, Imperial College London, Exhibition Road, London SW7 2AZ, England. *Correspondence e-mail: j.w.murray@imperial.ac.uk

The dual-function fructose-1,6/sedoheptulose-1,7-bisphosphatase (FBP/SBPase) in cyanobacteria carries out two activities in the Calvin cycle. Structures of this enzyme from the cyanobacterium *Synechocystis* sp. PCC 6803 exist, but only with adenosine monophosphate (AMP) or fructose-1,6-bisphosphate and AMP bound. The mechanisms which control both selectivity between the two sugars and the structural mechanisms for redox control are still unresolved. Here, the structure of the dual-function FBP/SBPase from the thermophilic cyanobacterium *Thermosynechococcus elongatus* is presented with sedoheptulose-7-phosphate bound and in the absence of AMP. The structure is globally very similar to the *Synechocystis* sp. PCC 6803 enzyme, but highlights features of selectivity at the active site and loop ordering at the AMP-binding site. Understanding the selectivity and control of this enzyme is critical for understanding the Calvin cycle in cyanobacteria and for possible biotechnological application in plants.

1. Introduction

The dual-function fructose-1,6/sedoheptulose-1,7-bisphosphatase (FBP/SBPase) plays a role in both the Calvin cycle and gluconeogenesis in cyanobacteria (Tamoi *et al.*, 1996, 1998, 1999). Disruption of the gene encoding the FBP/SBPase is lethal in both *Synechococcus* sp. PCC 7942 and *Synechocystis* sp. PCC 6803 (Tamoi *et al.*, 1999). FBP/SBPase is unique in that it catalyses two separate reactions in the Calvin cycle, both of which are catalysed by separate enzymes in plants. The reactions catalysed by FBP/SBPase are important for Calvin cycle flux, as indicated by their high predicted metabolic control coefficients (Poolman *et al.*, 2001). FBP/SBPase has been expressed in transplastomic tobacco (*Nicotiana tabacum*) and is shown to improve growth under certain circumstances (Miyagawa *et al.*, 2001). The dual-function FBP/SBPase is not regulated in the same way as the corresponding chloroplast enzymes (Tamoi *et al.*, 1998, 1999; Feng *et al.*, 2014). For this reason, the FBP/SBPase has also been the target of algicide screens (Sun *et al.*, 2014) aimed specifically at cyanobacteria. *Thermosynechococcus elongatus* is a thermophilic cyanobacterium which is used as a model organism for structural analysis of photosynthesis (Murray *et al.*, 2007).

The FBP/SBPase found in *T. elongatus* is a type II FBPase; a member of the larger Li$^+$-sensitive phosphatase superfamily. It shares 80% (277/347) sequence identity with the *Synechocystis* sp. PCC 6803 FBP/SBPase. *T. elongatus*, like
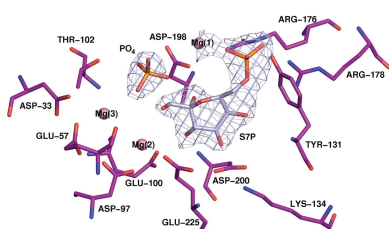
Table 1
Macromolecule-production information.

Source organism	*T. elongatus*
DNA source	*T. elongatus* genomic DNA
Forward primer	TTCCGCGTGGATCCGTGGATAACGTCATC
Reverse primer	CTGCAGATCTCGAGTTAGTACAGCTGG
Expression vector	pRSET A
Expression host	*E. coli* (KRX)
Complete amino-acid sequence of the construct produced	MRGSHHHHHHGLVPRGSMDNVIGLEIIEVVEQAA- IASARWMGKGDKNMADQAAVDAMRNRMNQIHM- RGRIVIGEGERDEAPMLYIGEEVGICTRPDAA- QYCNPEELIEIDIAVDPCEGTNLCAYGQPGSM- AVLAISEKGGLFAAPDFYMKKLAAPPAAKGKV- DIRNSATENLKILSECLDRAIDELVVVVMKRD- RHNDLIQEIRDAGARVQLISDGDVSAALACAF- SGTNIHALMGIGAAPEGVISAAAMRALGGHFQ- GQLVYDPAVVMTKEWANRTREGNLEELKKAGI- TDPDKVYEAEELASGETVLFAACGITPGMLMK- GVRFFKGGARTQSLVISTQSKTARFVDTIHMF- DQQLKSLQLY

Table 2
Crystallization.

Method	Hanging-drop vapour diffusion
Plate type	24-well plate
Temperature (K)	290
Protein concentration (mg ml^{-1})	15
Buffer composition of protein solution	50 mM Tris–HCl pH 7.9, 50 mM NaCl, 1 mM MgS7P, 0.2 M MgCl$_2$
Composition of reservoir solution	0.06 M Na HEPES pH 7.5, 0.12 M MgCl$_2$, 27%(v/v) PEG 400
Volume and ratio of drop	2 µl (1:1)
Volume of reservoir (µl)	100

Table 3
Data collection and processing.

Values in parentheses are for the outer shell.

Diffraction source	Beamline I04, Diamond Light Source
Wavelength (Å)	0.91730
Temperature (K)	100
Detector	Pilatus
Crystal-to-detector distance (mm)	326
Rotation range per image (°)	0.1
Total rotation range (°)	116
Exposure time per image (s)	0.1
Space group	$I4_122$
a, b, c (Å)	143.090, 143.090, 76.430
α, β, γ (°)	90.000, 90.000, 90.000
Resolution range (Å)	67.42–2.34 (2.40–2.34)
No. of unique reflections	17040 (1246)
Completeness (%)	99.95 (100)
Multiplicity	8.51 (8.52)
$\langle I/\sigma(I)\rangle$	22.4 (3.28)
R_{merge}	0.05 (0.63)
$CC_{1/2}$	99.9 (75.4)

and Arg314; Feng *et al.*, 2014). This AMP regulation differs from both GlpX, which is insensitive to AMP, and mammalian FBPases, in which AMP can bind directly to the active site (Xue *et al.*, 1994). In a sequence alignment, all key residues are identical between *T. elongatus* and *Synechocystis* sp. PCC 6803 for the cysteine disulfide bridge and AMP-regulatory region.

This paper presents the structure of the type II FBP/SBPase from *T. elongatus* bound with sedoheptulose-7-phosphate and in the absence of AMP.

2. Materials and methods

2.1. Macromolecule production

The full-length FBPase/SBPase gene (*tll1276*) was cloned downstream of a 6×His tag in a modified pRSET A vector encoding a thrombin cleavage site. Recombinant FBP/SBPase was expressed in *Escherichia coli* KRX cells and purified on a nickel-affinity column; the His tag was then cleaved at the thrombin site (MRGSHHHHHHGLVPRG/S) and the protein was maintained in 50 mM Tris–HCl buffer pH 7.9 with 50 mM NaCl. No further purification steps were necessary for crystallization. Macromolecule-production information is summarized in Table 1.

2.2. Crystallization

Purified FBP/SBPase was stored at 4°C and a stock concentration of 15 mg ml^{-1} was used for crystallization trials. In the crystallization condition 0.1 M HEPES pH 7.5, 0.8 M sodium dihydrogen phosphate, 0.8 M potassium dihydrogen phosphate, hexagonal bipyramidal crystals were found which were shown to belong to space group $P6_222$ or $P6_422$ but diffracted anisotropically to low resolution and were not processed further. Square bipyramidal crystals found in the condition in Table 2 [0.06 M Na HEPES pH 7.5, 0.12 M MgCl$_2$, 27%(v/v) PEG 400] diffracted to 2.3 Å resolution and were used for the structure presented here. 20%(v/v) glycerol was added to the mother liquor as a cryoprotectant. Sedoheptu-

Synechocystis sp. PCC 6803, is predicted to have both a type I (*tll0541*) and type II (*tll1276*) FBPase. After the *Synechocystis* sp. PCC 6803 FBP/SBPase, the most closely related protein for which there is a structure in the PDB is the class II FBPase GlpX from *Escherichia coli* (42% sequence identity). The cyanobacterial dual-function FBPases are not regulated by the same mechanisms as cytosolic and eukaryotic FBPases (regulated by AMP, insensitive to DTT) or chloroplastic FBPases (insensitive to AMP, activated by DTT), as they appear to be both activated by DTT and repressed by AMP (Feng *et al.*, 2014).

Both GlpX and the *Synechocystis* sp. PCC 6803 FBP/SBPase are compact globular proteins with two α/β-sandwich domains, but while GlpX is suggested to be active as a dimer (Brown *et al.*, 2009), the active state of the FBP/SBPase is thought to be tetrameric (Feng *et al.*, 2014). The active sites contain three metals; in the case of FBP/SBPase, these are three magnesium ions. The *Synechocystis* sp. PCC 6803 FBP/SBPase has both an allosteric AMP-binding site and a suggested disulfide bridge (Cys75–Cys99) which might account for dithiothreitol (DTT) sensitivity (Feng *et al.*, 2014), but this disulfide was not observed in the structure and is at an unfeasible distance, with the two thiol groups over 28 Å from one another in crystallographic models (PDB entries 3rpl and 3roj; Feng *et al.*, 2014). The *Synechocystis* sp. PCC 6803 FBP/SBPase protein is a biologically active tetramer and residues from two adjacent monomers contribute to the AMP-binding regulatory domain (Arg164, Asn213, His215, Arg307, Phe309

Table 4
Structure refinement.

Values in parentheses are for the outer shell.

Resolution range (Å)	67.4–2.34 (2.49–2.34)
Completeness (%)	99.88 (100)
No. of reflections, working set	16166 (2645)
No. of reflections, test set	862 (151)
Final R_{cryst}	0.166 (0.206)
Final R_{free}	0.224 (0.290)
No. of atoms	
Protein	2537
Ion	8
Ligand	18
Water	74
Total	2637
R.m.s. deviations	
Bonds (Å)	0.007
Angles (°)	1.054
Ramachandran plot	
Favoured (%)	98
Additionally allowed (%)	2
Outliers (%)	0
MolProbity score	1.30 [100th percentile at 2.34 ± 0.25 Å resolution]

lose-7-phosphate (magnesium salt; MgS7P) was added to the hanging drop at a concentration of 1 m*M* for co-crystallization studies.

2.3. Data collection and processing

Data were collected under cryocooled conditions on beamline I04 at the Diamond Light Source. All images from the synchotron were processed by *xia*2 (Winter, 2009) using the 3dii setting/*XDS* (Kabsch, 2010). Data-collection and processing statistics are presented in Table 3.

2.4. Structure solution and refinement

The structure was solved by molecular replacement using *Phaser* (McCoy *et al.*, 2005) with *E. coli* GlpX in complex with fructose-1,6-phosphate (PDB entry 2r8t; Brown *et al.*, 2009) as the model. Structures were refined using *REFMAC* (Murshudov *et al.*, 2011) and tools from the *CCP*4 package (Winn *et al.*, 2011) and were finished in *PHENIX* (Adams *et al.*, 2010). Model building was performed in *Coot* (Emsley & Cowtan, 2004). *MolProbity* was used for validation (Chen *et al.*, 2010). Structure-solution and refinement statistics are presented in Table 4.

3. Results and discussion

The crystals belonged to space group $I4_122$. The asymmetric unit contains a monomer, with a solvent content of 53%. All loop regions are visible in the structure and are resolved, with the exception of ten residues at the C-terminus which are structured in the cyanobacterial dual-function FBP/SBPase structure with AMP bound. The structure appears to be an adventitiously purified product complex, as not only is the sedoheptulose-7-phosphate visible but an additional phosphate close to the C_1 position of the sugar is also visible in the electron density at the active site. In contrast to previous

cyanobacterial structures, no adenine mononucleotide phosphate (AMP) is bound, and the C-terminal tail that binds AMP is not visible in the electron density.

Superposition of C^α atoms of the structure of the *Synechocystis* sp. PCC 6803 FBP/SBPase bound with fructose-1,6-bisphosphate and AMP (PDB entry 3rpl) and the *T. elongatus* structure bound with sedoheptulose-7-phosphate (PDB entry 5a5l) shows a root-mean-square deviation (r.m.s.d.) of 0.727 Å. The two structures are very similar. This value changes to 0.740 Å for the comparison with the *Synechocystis* structure without the sugar substrate bound (PDB entry 3roj), implying that the binding of the substrate does not result in any global conformational change. Both proteins show the two α/β-sandwich domains of the Li$^+$-sensitive phosphatases.

All active-site residue identities (Asp33, Glu57, Glu100, Thr102, Tyr131, Lys134, Arg176, Arg178, Asp198, Asp200 and Glu225) and positions are conserved between the *Synechocystis* sp. PCC 6803 structure and the *T. elongatus* structure bound with different sugars. The metals (magnesium ions) are
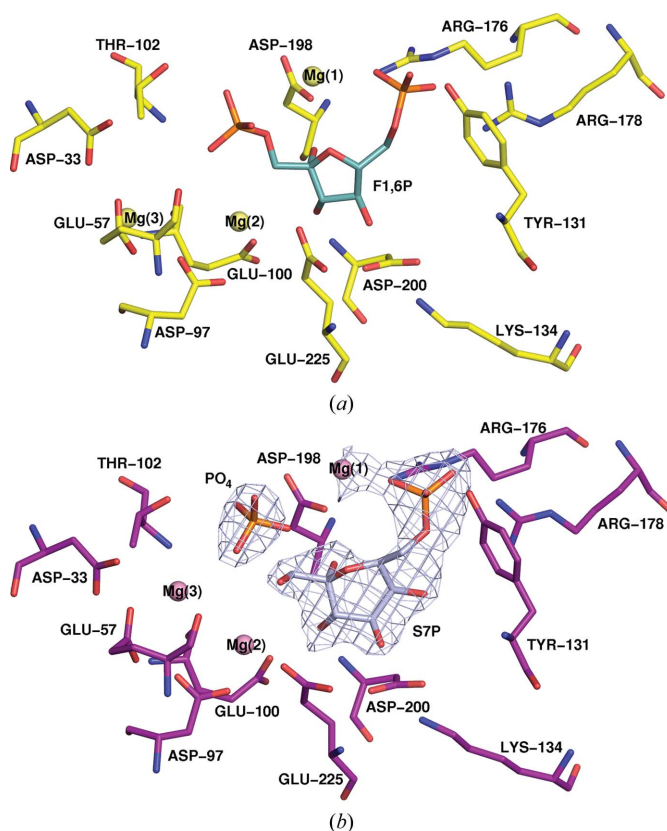
Figure 1
Comparison of similar active sites. (*a*) *Synechocystis* sp. PCC 6803 structure (PDB entry 3rpl, yellow) shown with key active-site residues shown as sticks (Asp33, Glu57, Glu100, Thr102, Tyr131, Lys134, Arg176, Arg178, Asp198, Asp200 and Glu225). (*b*) *T. elongatus* structure (PDB entry 5a5l, purple) bound with sedoheptulose-7-phosphate (lavender) with equivalent active-site residues shown as sticks (Asp33, Glu57, Glu100, Thr102, Tyr131, Lys134, Arg176, Arg178, Asp198, Asp200 and Glu225). Magnesium ions are shown as spheres. The phosphate (PO$_4$) of the suggested product complex is clearly visible. Ligand OMIT map difference density is shown for the S7P ligand and phosphate (lavender mesh) using a 4σ contour level. Active-site residues and metals are in the same conformation; selectivity between the sugars is not the result of large-scale conformational change.

shifted by 1.9, 2.0 and 3.4 Å, respectively, for magnesiums 1, 2 and 3 (Fig. 1) in the two structures but are bound to the same residues. The phosphate in the *T. elongatus* structure suggests that the product complex has been purified as it resides roughly at the equivalent '1' position of the fructose-1,6-bisphosphate and is located next to the C1 atom of sedoheptulose-7-phosphate. There does not appear to be a structural mechanism to differentiate between sugars.

Redox regulation is thought to be important for type II FBPases involved in photosynthesis (Feng *et al.*, 2014). The mechanism of redox regulation in cyanobacterial FBP/SBPases is clearly distinct from that in FBPase structures from the higher plant *Pisum sativum* (PDB entries 1d9q and 1dbz; Chiadmi *et al.*, 1999), in which the redox-active disulfide is on a loop covering the active site. Feng and coworkers suggest that cysteines at positions Cys75 and Cys99 may rearrange to form a disulfide bond in the inactive enzyme state using evidence from a targeted mutagenesis activity assay (Feng *et al.*, 2014). In both the *T. elongatus* structure and the *Synechocystis* sp. PCC 6803 structure the only oxidized disulfide bond appears to be Cys75–Cy84. Our structure does not provide evidence for the hypothesis of Feng and coworkers, as the two residues are too far apart in this conformation and would require significant conformational change to the 'inactive' state. In an
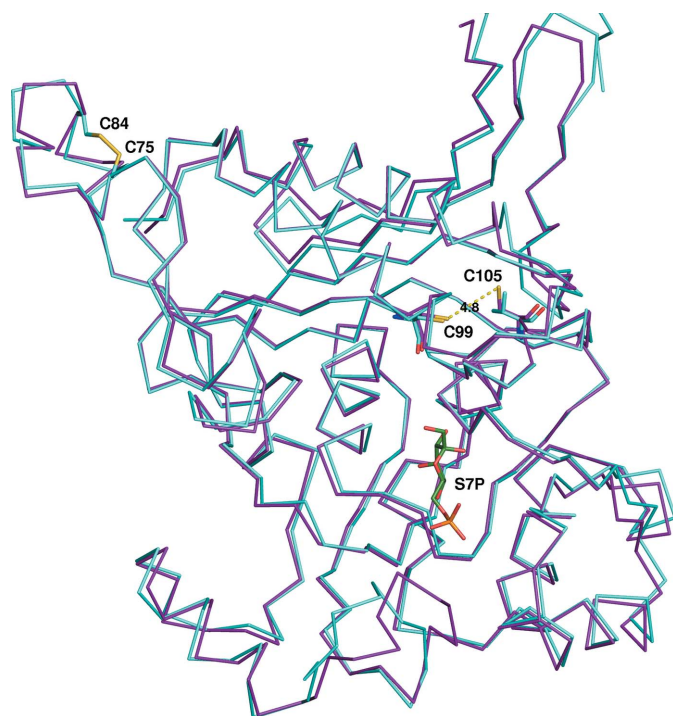
alignment of the *T. elongatus* FBP/SBPase and the *Synechocystis* sp. PCC 6803 FBP/SBPase all cysteines were conserved in both position and structural orientation, with four exceptions: Cys235, Cys281 and Cys288 were not present in *T. elongatus* and Cys105 was not present in *Synechocystis* sp.
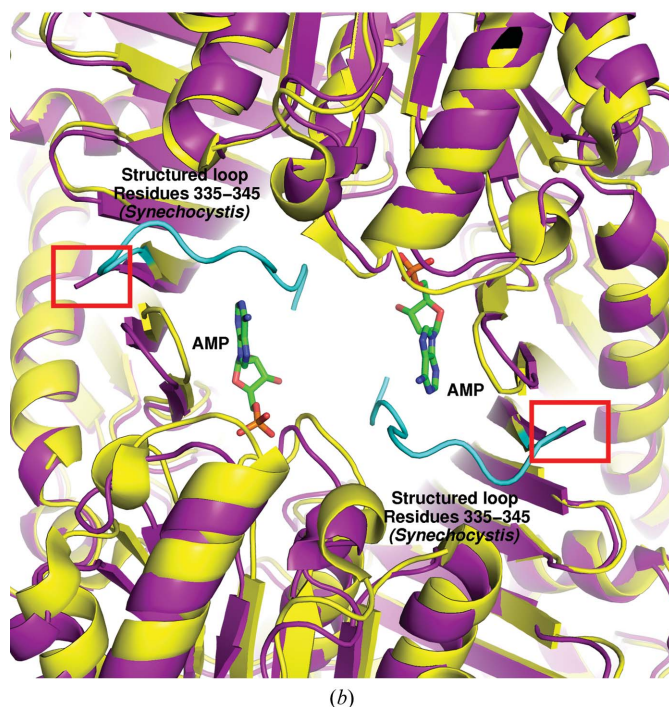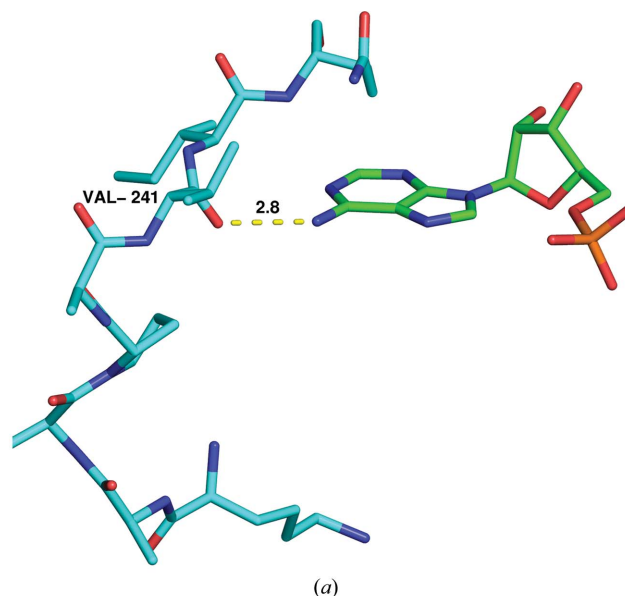
(a)

(b)

Figure 3
The AMP-binding loop found in the *Synechocystis* sp. PCC 6803 structure is not visible in the *T. elongatus* electron density in the absence of AMP. (a) Stick model of *Synechocystis* sp. PCC 6803 residues 335–345 (cyan), which form a structured loop in the presence of AMP (green). The backbone carboxyl of Val341 forms a hydrogen bond to AMP. (b) AMP (green) is bound only in the *Synechocystis* sp. PCC 6803 structure (yellow cartoon). The final ten residues (structured loop) of the *Synechocystis* sp. PCC 6803 structure are shown in cyan as in (a) to indicate that they form part of the AMP-binding region. The purple cartoon is the *T. elongatus* FBP/SBPase. The red box indicates the end of the *T. elongatus* structure, as the final residues are not visible in the electron density.

Figure 2
Redox regulation. The residues previously identified as being important for redox regulation in *Synechocystis* sp. PCC 6803 (cyan) are Cys75 and Cys99, which are too far away to be involved in a disulfide bond in the current conformation. Cys75 and Cys84 are oxidized in both structures. In addition, Cys105 could potentially form a disulfide bond with Cys99 in the *T. elongatus* protein (dashed line, 4.8 Å). This Cys105 is not conserved and is a valine in the *Synechocystis* protein. Sedoheptulose-7-phosphate (S7P, green) is shown in the image to highlight the distance of these residues from the active site. The *T. elongatus* structure is shown as a ribbon (purple).

PCC 6803. The cysteines at positions Cys75, Cys84 and Cys99 are well conserved in a survey of cyanobacterial FBP/SBPase sequences. In the *T. elongatus* sequence Cys105 is positioned sufficiently close to Cys99 to form a disulfide bond (see Fig. 2) but is not oxidized in this structure, and this cysteine is not generally conserved in cyanobacteria. In conclusion, no structural evidence for the rearrangement hypothesis of Feng and coworkers can be seen in our structure lacking AMP (Feng *et al.*, 2014).

The AMP-binding domain has key residues Arg164, Asn213, His215, Arg307, Phe309 and Arg314 in the *Synechocystis* sp. PCC 6803 structure (Feng *et al.*, 2014). All of the key residues identified are conserved in our sequence and are almost identical in both position and orientation in the structure. One critical difference appears to be the ordering of the final residues of the C-terminus. Phe337 is the final residue that is visible in the electron density of the *T. elongatus* structure. Feng and coworkers reported that the *Synechocystis* sp. PCC 6803 enzyme would not crystallize in the absence of AMP. This is presumably because this region (see Fig. 3, cyan) was unstructured and disrupted crystallization. While the full sequence of the loops is not well conserved, there is a clear hydrogen-bonding interaction between the backbone carboxyl of Val341 and the nitrogenous base (the amino group extending from the C6 atom of the adenine moiety), which is not resolved in our structure.

The main contribution of this structure, which is globally very similar to the *Synechocystis* sp. PCC 6803 enzyme, is the evidence for disorder of the AMP-binding region in the absence of AMP. In addition, the structure provides further information for understanding selectivity at the active site and supports the assertion that the mechanism of redox regulation is not yet structurally evident.

Acknowledgements

References

Adams, P. D. *et al.* (2010). *Acta Cryst.* D**66**, 213–221.

Brown, G., Singer, A., Lunin, V. V., Proudfoot, M., Skarina, T., Flick, R., Kochinyan, S., Sanishvili, R., Joachimiak, A., Edwards, A. M., Savchenko, A. & Yakunin, A. F. (2009). *J. Biol. Chem.* **284**, 3784–3792.

Chen, V. B., Arendall, W. B., Headd, J. J., Keedy, D. A., Immormino, R. M., Kapral, G. J., Murray, L. W., Richardson, J. S. & Richardson, D. C. (2010). *Acta Cryst.* D**66**, 12–21.

Chiadmi, M., Navaza, A., Miginiac-Maslow, M., Jacquot, J.-P. & Cherfils, J. (1999). *EMBO J.* **18**, 6809–6815.

Emsley, P. & Cowtan, K. (2004). *Acta Cryst.* D**60**, 2126–2132.

Feng, L., Sun, Y., Deng, H., Li, D., Wan, J., Wang, X., Wang, W., Liao, X., Ren, Y. & Hu, X. (2014). *FEBS J.* **281**, 916–926.

Kabsch, W. (2010). *Acta Cryst.* D**66**, 125–132.

McCoy, A. J., Grosse-Kunstleve, R. W., Storoni, L. C. & Read, R. J. (2005). *Acta Cryst.* D**61**, 458–464.

Miyagawa, Y., Tamoi, M. & Shigeoka, S. (2001). *Nature Biotechnol.* **19**, 965–969.

Murray, J. W., Maghlaoui, K. & Barber, J. (2007). *Acta Cryst.* F**63**, 998–1002.

Murshudov, G. N., Skubák, P., Lebedev, A. A., Pannu, N. S., Steiner, R. A., Nicholls, R. A., Winn, M. D., Long, F. & Vagin, A. A. (2011). *Acta Cryst.* D**67**, 355–367.

Poolman, M. G., Ölçer, H., Lloyd, J. C., Raines, C. A. & Fell, D. A. (2001). *Eur. J. Biochem.* **268**, 2810–2816.

Sun, Y., Zhang, R., Li, D., Feng, L., Wu, D., Feng, L., Huang, P., Ren, Y., Feng, J., Xiao, S. & Wan, J. (2014). *J. Chem. Inf. Model.* **54**, 894–901.

Tamoi, M., Ishikawa, T., Takeda, T. & Shigeoka, S. (1996). *Arch. Biochem. Biophys.* **334**, 27–36.

Tamoi, M., Murakami, A., Takeda, T. & Shigeoka, S. (1998). *Biochim. Biophys. Acta*, **1383**, 232–244.

Tamoi, M., Takeda, T. & Shigeoka, S. (1999). *Plant. Cell. Physiol.* **40**, 257–261.

Winn, M. D. *et al.* (2011). *Acta Cryst.* D**67**, 235–242.

Winter, G. (2009). *J. Appl. Cryst.* **43**(1), 186–190.

Xue, Y., Huang, S., Liang, J.-Y., Zhang, Y. & Lipscomb, W. N. (1994). *Proc. Natl Acad. Sci. USA*, **91**, 12482–12486.